Journal of Power Sources 253 (2014) 251–255

Contents lists available at ScienceDirect

Journal of Power Sources

journal homepage: www.elsevier.com/locate/jpowsour

Short communication

Hydrothermal synthesis and potential applicability of rhombohedral siderite as a high-capacity anode material for lithium ion batteries

Shiqiang Zhao, Yue Yu, Shanshan Wei, Yuxi Wang, Chenhao Zhao, Rui Liu, Qiang Shen*

Key Laboratory for Colloid and Interface Chemistry of Education Ministry, School of Chemistry and Chemical Engineering, Shandong University, Jinan 250100, China

HIGHLIGHTS

- $FeCO_3$ micro-rhombohedra are uniquely obtained via a hydrothermal route.
- Synthetic siderite can serve as a high-capacity lithium ion battery anode.
- The 120th discharge capacity is as high as 1018 mAh g^{-1} at 200 mA g^{-1}.
- The excellent lithium storage capability of $FeCO_3$ has been investigated.

ARTICLE INFO

Article history:
Received 8 October 2013
Received in revised form
28 November 2013
Accepted 12 December 2013
Available online 19 December 2013

Keywords:
Lithium ion battery
Anode material
Hydrothermal synthesis
Ferrous carbonate
Rhombohedral crystallite

ABSTRACT

Natural siderite is a valuable iron mineral composed of ferrous carbonate ($FeCO_3$), which is commonly found in hydrothermal veins and contains no sulfur or phosphorus. In this paper, micro-sized $FeCO_3$ crystallites are synthesized via a facile hydrothermal route, and almost all of them possess a rhombohedral shape similar to that of natural products. When applied as an anode material for lithium ion batteries, the synthetic siderite can deliver an initial specific discharge capacity of ~1587 mAh g^{-1} with a coulombic efficiency of 68% at 200 mA g^{-1}, remaining a reversible value of 1018 mAh g^{-1} over 120 cycles. Even at a high current density of 1000 mA g^{-1}, after 120 cycles the residual specific capacity (812 mAh g^{-1}) is still higher than the theoretical capacity of $FeCO_3$ (463 mAh g^{-1}). Moreover, a novel reversible conversion mechanism accounts for the excellent electrochemical performances of rhombohedral $FeCO_3$ to a great extent, implying the potential applicability of synthetic siderite as lithium ion battery anodes.

1. Introduction

Lithium ion battery (LIB) is one of the most promising energy storage devices, due to its high-capacity and high-power properties [1,2]. Thus, the exploration or development of an electrode material with low cost, facile preparation and excellent safety has become a hot research topic [1,3,4], such as that of natural graphite or artificially synthesized nanostructured carbons. As for transition metal oxysalts (e.g., oxalate and carbonate) applied as LIB anodes [5–15], the observed high-performance features arouse us to further investigate the controversial lithium storage mechanisms and a possible structure–function relationship for practical purposes.

According to the well-accepted lithium storage mechanism of transition metal oxysalts reported in literature [16], the lithiation–delithiation process can be similarly assigned to a reversible conversion between transition metal oxysalt and transition metal. Up to date, it is still ambiguous to know the exact reason why the always observed reversible capacity (or capacity retention) is higher than the theoretical value calculated from electrochemical reactions [6,8,9]. For example, the theoretical capacities of $MnCO_3$ and CoC_2O_4 are 466 and 365 mAh g^{-1}, while the corresponding reversible values can reach 750 (2nd cycle, at C/4, C = 1 Li h^{-1} mol^{-1}) and 900 mAh g^{-1} (40th cycle, at 2C), respectively [6,8]. It has been proved that the extra capacity could be ascribed to the capacitive contribution of Faradic and non-Faradic reasons [6,8,17,18]. By comparing the theoretical capacity of chemical formula $CoCO_3$ (451 mAh g^{-1}) with the detected reversible capability of synthetic $CoCO_3$ microcubes (~900 mAh g^{-1}), a plausible catalytic conversion mechanism has been proposed: the reversible redox reaction between C^{4+} in CO_3^{2-} and its low valence states (e.g., C^{2+} and C^0) under the catalysis of metallic nanoparticles [9,19]. Although the alkali metal carbonates (e.g., Li_2CO_3 and Na_2CO_3) are inactive for lithium storage, the continuous discharge–charge

* Corresponding author. Tel.: +86 531 88361387; fax: +86 531 88364464.
E-mail address: qshen@sdu.edu.cn (Q. Shen).

0378-7753/$ – see front matter © 2013 Elsevier B.V. All rights reserved.
http://dx.doi.org/10.1016/j.jpowsour.2013.12.055

cycling of $CoCO_3$ can induce the formation of Li_2CO_3 and Li_2O in sequence [15,19,20]. Furthermore, to explain the high-capacity feature of $CoCO_3$–polypyrrole composites [15], the similar two-step conversion mechanism has been further proved, shown as below.

$$CoCO_3 + 2Li \leftrightarrow Co + Li_2CO_3 \quad (1)$$

$$Li_2CO_3 + (4 + 0.5x)Li \leftrightarrow 3Li_2O + 0.5(Li_xC_2) \quad (x = 0, 1, 2) \quad (2)$$

In fact, siderite $FeCO_3$ is a low-cost and nontoxic transition metal carbonate in comparison with $CoCO_3$ and $MnCO_3$, which is a valuable iron mineral found in hydrothermal veins [21]. Rambutan-like $FeCO_3$ nanostructures, i.e., the hollow microspheres composed of ~7.2 nm nanofibers, have been applied as LIB anodes recently, possessing a high reversible capacity of ~710 mAh g^{-1} over 200 cycles at 200 mA g^{-1} [14]. Aroused by this, herein the hydrothermally synthesized $FeCO_3$ micro-rhombohedra are also used as anode active substances, amazingly exhibiting the 120th specific discharge capacity of 1018 mAh g^{-1} at 200 mA g^{-1}. These should relate to a novel electrochemical reaction mechanism of $FeCO_3$ towards metal lithium, which will be discussed in details in context.

2. Experimental

2.1. Synthesis of rhombohedral $FeCO_3$

All the chemicals are of analytic grade and ultrapure water (18.2 MΩ cm) was used throughout the solution preparation. Firstly, solid-state ferrous sulfate heptahydrate $FeSO_4 \cdot 7H_2O$ (1.0 mmol), ammonium carbonate $(NH_4)_2CO_3$ (5.0 mmol) and ascorbic acid (1.0 mmol) were sequentially added into ultrapure water (40.0 mL) under stirring at room temperature. Secondly, the resulting suspension was transferred into a 50-mL Teflon-lined autoclave, which was sealed and allowed to stand still in a thermostatic chamber at 160 °C for 15 h. Finally, the autoclave was cooled to room temperature, and the precipitates were collected by centrifugation, washed with ultrapure water then absolute alcohol for 3 times and then dried at 80 °C for 10 h.

2.2. Structural characterization

X-ray diffraction (XRD) measurements were performed using a Rigaku D/max-2400 powder X-ray diffractometer with Cu-Kα radiation (40 kV, 120 mA), and a 0.08° step (25 s) and the 2θ range of 10–80° were selected to analyze crystal phase. Samples were Pt-coated prior to examination using a JEOL JSM-6700F scanning electron microscope (SEM), fitted with a field emission source and operating at an accelerating voltage of 15 kV. X-ray photoelectron spectroscopy (XPS) measurements were performed on a VG Scientific ESCALAB 220i-XL electron spectrometer using Al Kα radiation.

2.3. Electrochemical measurements

After dispersing the rhombohedral $FeCO_3$, acetylene black and sodium alginate at a weight ratio of 80:10:10 in ultrapure water, the resulting homogeneous slurry was pasted onto a pure copper foil and dried at 80 °C for 12 h. And then, the foil was cut into discs (12 mm in diameter) and used as working electrodes with a loading density of 2.2 ± 0.4 mg cm^{-2}. Lithium metal, nickel foam, glass fibers and commercial LBC 305-01 $LiPF_6$ solution (Shenzhen Xinzhoubang) were used as counter electrode, current collector, separator and electrolyte, respectively. CR2032-type coin cells were assembled in an argon-filled glove box.

Galvanostatic cycling tests were conducted on an LAND CT2001A system (Wuhan Landian) in the voltage range of 0.01–3.0 V (vs. Li^+/Li and the same below). Cyclic voltammetry (CV) measurements were performed on an LK 2005A Electrochemical Workstation (Tianjin Lanlike) within the potential range of 0.01 and 3.0 V at 0.1 mV s^{-1}. To investigate the reaction mechanism of $FeCO_3$ with lithium, galvanostatic cycling tests were stopped at an appropriate time and cells were unpacked in an air-atmosphere

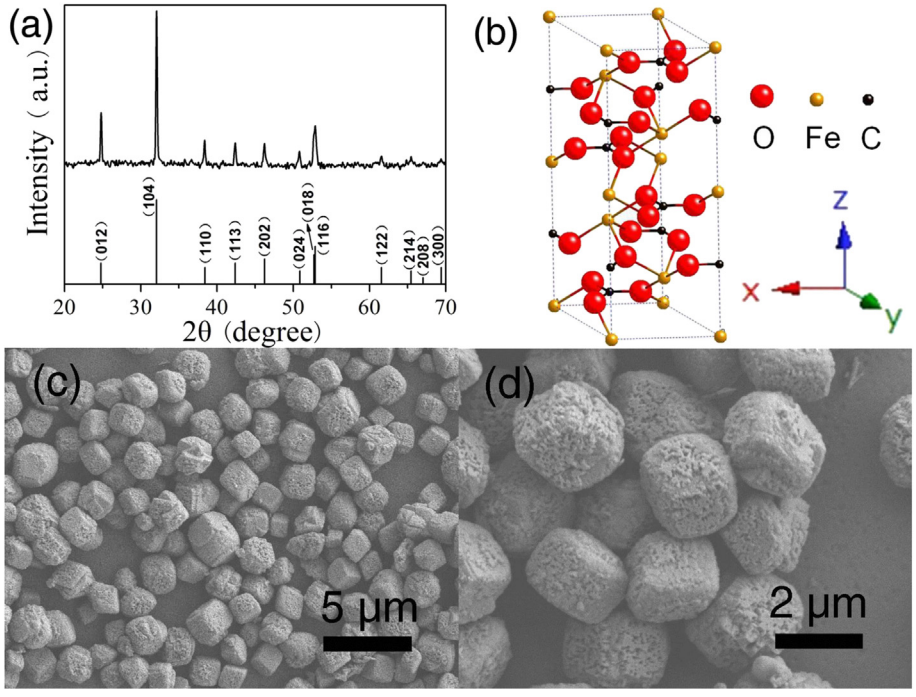

Fig. 1. (a) XRD pattern, (b) unit cell scheme and (c, d) SEM images of $FeCO_3$ rhombohedra obtained via a hydrothermal route.

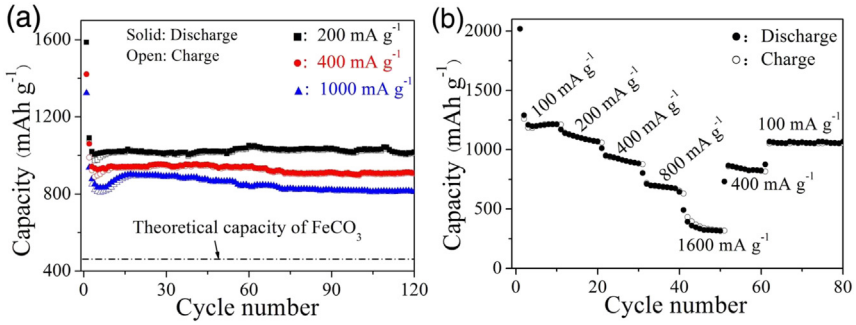

Fig. 2. (a) Cycling stability and (b) high-rate performance of rhombohedral $FeCO_3$ electrodes operated at different current densities.

ventilating cabinet. And then, the anode active substances were quickly washed with a sufficient amount of ethanol, dried at 80 °C for 12 h, and used for XPS measurements.

3. Results and discussion

In crystallography, crystalline $FeCO_3$ is isostructural with the thermodynamically stable phase of anhydrous calcium carbonate (i.e. calcite), belonging to the hexagonal system and the D_{3d}^6 space group ($R\bar{3}C$). As far as the synthesis procedure is concerned, siderite, there is no cationic substitutes for the iron (II) of hydrothermal product, the corresponding XRD pattern (Fig. 1a) should coincide with the standard data of rhombohedral $FeCO_3$ crystals (a = 4.69 Å; c = 15.37 Å; JCPDS No. 12-0531). According to the schematic drawing of a unit cell of crystalline $FeCO_3$ (Fig. 1b), each Fe atom and its 6 adjacent O atoms from different CO_3^{2-} groups construct a FeO_6 octahedron. Also, each C atom and its 3 adjacent O atoms at the same plane form a CO_3 equilateral triangle, which is perpendicular to the z-axis. Resembling the structure of crystalline siderite, the synthetic sample is rhombohedral in shape and possesses 6 striated faces.

SEM observation displays that the hydrothermally obtained samples are rhombohedral crystallites (Fig. 1c). By statistic analysis, these rhombohedra give an average size of 1.4 ± 0.2 μm. Furthermore, Fig. 1d clearly shows that each $FeCO_3$ micro-particles possess 6 rough faces. This is in agreement with the fact that natural siderite rhombohedra generally possess curved and/or striated faces outside. Probably, both the synthetic and natural rhombohedra are aggregates composed of tiny nanoparticles.

When the synthetic siderite is tentatively applied as an LIB anode, within 0.01 and 3 V the plots of discharge–charge capacities against cycle numbers are shown in Fig. 2a. At a current density of 200, 400 or 1000 mA g^{-1}, the as-prepared $FeCO_3$ micro-rhombohedra can demonstrate a high initial discharge capacity of ~1587, 1421 or 1324 mAh g^{-1} and a high coulombic efficiency of ~68%, 70% or 71%. It is well-known that the initial capacity loss can be attributed to the formation of solid electrolyte interface (SEI) films and/or electrolyte degradation [22]. Fig. 2a further presents the 120th reversible capacities of 1018, 909 and 812 mAh g^{-1} at the current rates of 200, 400 and 1000 mA g^{-1}. That is, even at 1000 mA g^{-1} the residual value is much higher than the theoretical capacity of $FeCO_3$ (~463 mAh g^{-1}). According to literature results [6,9,14], the 25th discharge capacity of $MnCO_3$ is ~450 mAh g^{-1} at C/4, the 40th reversible value of graphene-doped $CoCO_3$ is ca. 744 mAh g^{-1} at 200 mA g^{-1}, and the 200th discharge capacity of hollow-spherical $FeCO_3$ is as high as 710 mAh g^{-1} at 200 mA g^{-1}. Therefore, the electrochemically cycling stability of rhombohedral $FeCO_3$ is excellent.

Fig. 2b shows the rate performance of a rhombohedral $FeCO_3$ electrode cycled within the potential range of 0.01 and 3 V. The observed discharge capacity (or charge capacity) gradually decreases with the increasing current rate from 100 to 1600 mA g^{-1}. Upon cycling, the average coulombic efficiencies are estimated to be ~99 and ~100% at 400 and 1600 mA g^{-1}, respectively. Also shown in Fig. 2b, when current density returns from 1600 to 400 mA g^{-1}, the corresponding discharge capacity recovers from 314.6 (the 50th cycle) to 866.5 mAh g^{-1} (the 52nd cycle). These, together with the high cycling performance shown in Fig. 2a, suggest a novel electrochemical reaction mechanism of the synthetic siderite towards metal lithium.

To deal with the electrochemical reactivity of $FeCO_3$, at the current density of 200 mA g^{-1} parts of the voltage profiles are shown in Fig. 3a, and at a scanning rate of 0.1 mV s^{-1} the CV behaviors of a $FeCO_3$ electrode are shown in Fig. 3b. During the 1st discharging process, the open-circuit potential (~2.2 V) decreases sharply to 0.57 V, followed by a long voltage plateau around ~0.5 V (Fig. 3a). Correspondingly, there appears a wide CV peak in the voltage range of 0.75–0.20 V in the 1st cathodic process (Fig. 3b).

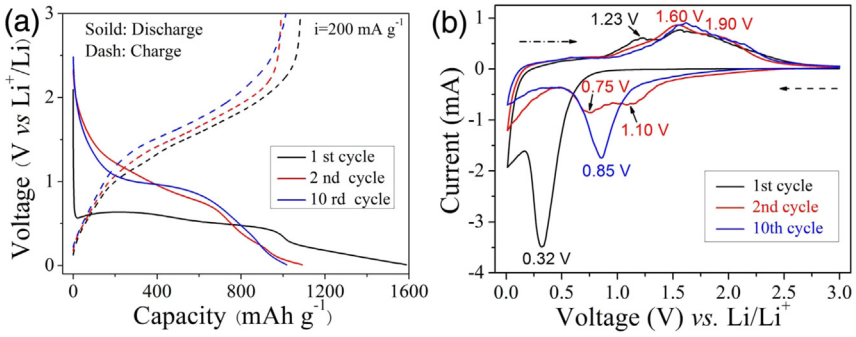

Fig. 3. (a) Representative discharge–charge voltage profiles and (b) cyclic voltammetry (CV) curves of $FeCO_3$/Li cell operated at 200 mA g^{-1} and scanned at 0.1 mV s^{-1}, respectively.

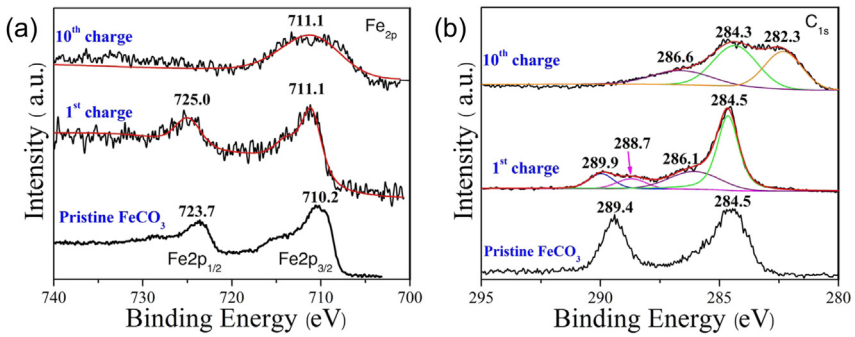

Fig. 4. XPS spectra of (a) Fe_{2p} and (b) C_{1s} for pristine $FeCO_3$ and its electrochemical cycled products.

This indicates both the formation of SEI films and the lithiation of $FeCO_3$ rhombohedra [9,18,22], and the initial electrochemical reaction of $FeCO_3$ with Li can be simply described as the Equation (3).

$$FeCO_3 + 2Li^+ + 2e^- \rightarrow Fe + Li_2CO_3 \quad (3)$$

There is no clear voltage plateau in the 1st galvanostatic charging process (Fig. 2a), however, there are two CV peaks and a shoulder in the 1st anodic process (Fig. 2b). As shown in Fig. 2b, the peak at ~1.60 V and its wide shoulder around 1.90 V may be successively assigned to the gradual change in iron oxidation state (i.e., $Fe^0 \rightarrow Fe^{2+} \rightarrow Fe^{3+}$) [23,24], while the current intensity of another peak (~1.23 V) gradually decreases along with the continuous potential scanning and then completely disappears in the 10th anodic process. As far as we know, the CV peak at ~1.23 V in the 1st anodic process is presently unknown, which needs to be further conducted.

Also shown in Fig. 2b, there appear two peaks at ~1.10 and ~0.75 V for the 2nd cathodic process, corresponding to the reverse change in iron oxidation state (i.e., $Fe^{3+} \rightarrow Fe^{2+} \rightarrow Fe^0$). In the 10th galvanostatic discharging process, a clear and stable voltage plateau at ~1.0 V can be observed (Fig. 2a), corresponding to the lonely CV peak at ~0.85 V in the 10th anodic process (Fig. 2b). It should be mentioned that, after the 10th cathodic–anodic cycle, subsequent CV curves have almost no shape changes (Data omitted) and indicate reversible redox reactions thereafter.

To clarify the novel electrochemical activity of rhombohedral $FeCO_3$ towards metal Li, parts of the cycled Li/$FeCO_3$ cells are unpacked, and the corresponding products are measured using XPS method. For a comparison purpose, XPS profiles of pristine $FeCO_3$ and its electrochemical derivatives collected shortly after the 1st and 10th discharge–charge cycles are presented in Fig. 4. XPS result of as-prepared $FeCO_3$ coincides well with that of the commonly accepted standard as reported, clearly showing both the original Fe 2p (i.e., $2p_{3/2}$ ~ 710.2 eV and $2p_{1/2}$ ~ 723.7 eV) peaks (Fig. 4a) and the redefined C_{1s} peaks at 284.5 and 289.4 eV (Fig. 4b), respectively [25].

As shown in Fig. 4a, after the initial discharge–charge cycle the Fe $2p_{3/2}$ and $2p_{1/2}$ peaks of pristine $FeCO_3$ experience a slight shift to 711.1 and 725.0 eV, respectively. Rapidly after the 10th cycle, XPS measurement of the cycled $FeCO_3$ merely displays the Fe $2p_{3/2}$ peak at 711.1 eV, indicating both the complete lithiation of micro-sized rhombohedra and the formation of unknown Fe^{3+}-based derivatives [26]. In Fig. 4b, the C_{1s} XPS characteristics of different C-containing groups are also marked therein [9,27,28]: C–C, at 284.3 or 284.5 eV; CO_3^{2-} in $FeCO_3$ or Li_2CO_3, at 289.4/289.9 or 288.7 eV; C=O/C–F, at 286.1 or 286.6 eV; and Li_2C_2 (or LiC), at 282.3 eV. Aside from the surface behaviors of conductive additive acetylene black and polymeric binder, the detailed measurements of cycled $CoCO_3$ suggest a novel electrochemical activity of $FeCO_3$ towards metallic Li [9,15,20,29].

In comparison with the theoretical capacity of $FeCO_3$ (463 mAh g^{-1}), the electrochemical oxidation of Fe^0 to Fe^{3+} merely corresponds to a relatively high value of 694 mAh g^{-1}. Namely, this can hardly explain the practical capacity of ~1000 mAh g^{-1} operated at 200 mA g^{-1}. Basing on the results listed above, the extremely high capacity of rhombohedral $FeCO_3$ may be attributed to the following aspects: (i) an initially incomplete reversible reaction for the generation of Fe and Li_2CO_3; (ii) the subsequently reversible redox reaction of $Fe^0 \leftrightarrow Fe^{3+}$; (iii) the simultaneous reversible redox reactions between high-valence (e.g., C^{4+} in Li_2CO_3 and sodium alginate) and low-valence C (e.g., C^0 in acetylene black and C^{-1} in Li_2C_2); (iv) the capacitive contribution of surface charge storage.

4. Conclusions

Rhombohedral $FeCO_3$ (or synthetic siderite) has been facilely synthesized by a hydrothermal method, possessing an average size of 1.4 ± 0.2 μm. Tentatively applied as LIB anodes, the excellent durability and high-rate performance of these micro-rhombohedra can be reproducibly observed. Even at 1000 mA g^{-1}, the reversible capacity (~800 mAh g^{-1}) is still higher than the theoretical capacity of $FeCO_3$ (463 mAh g^{-1}). As for the novel electrochemical activity of $FeCO_3$ towards metal lithium, the simultaneous formation of unknown Fe^{3+}-containing derivatives and possible C^{-1}-containing Li_2C_2 incompletely answers the high-capacity characteristics of $FeCO_3$ (e.g., the 120th reversible value ~1000 mAh g^{-1} at 200 mA g^{-1}). Therefore, the lithium storage mechanism of $FeCO_3$ needs to be further conducted in future.

Acknowledgments

The authors thank the financial supports from Shandong Province (ZR2012BM001) and from the National Basic Research Program of China (2011CB935900).

References

[1] P.G. Bruce, B. Scrosati, J.-M. Tarascon, Angew. Chem. Int. Ed. 47 (2008) 2930.
[2] B. Scrosati, J. Hassoun, Y.-K. Sun, Energy Environ. Sci. 4 (2011) 3287.
[3] M. Armand, J.M. Tarascon, Nature 451 (2008) 652.
[4] Y.G. Guo, J.S. Hu, L.J. Wan, Adv. Mater. 20 (2008) 2878.
[5] M.J. Aragón, C.P. Vicente, J.L. Tirado, Electrochem. Commun. 9 (2007) 1744.
[6] M.J. Aragón, B. León, C.P. Vicente, J.L. Tirado, J. Power Sources 196 (2011) 2863.
[7] S. Mirhashemihaghighi, B. Leon, C.P. Vicente, J.L. Tirado, R. Stoyanova, M. Yoncheva, E. Zhecheva, R.S. Puche, E.M. Arroyo, J.R. de Paz, Inorg. Chem. 51 (2012) 5554.
[8] M.J. Aragón, B. León, C.P. Vicente, J.L. Tirado, A.V. Chadwick, A. Berko, S.-Y. Beh, Chem. Mater. 21 (2009) 1834.
[9] L. Su, Z. Zhou, X. Qin, Q. Tang, D. Wu, P. Shen, Nano Energy 2 (2013) 276.

[10] M.C. López, J.L. Tirado, C.P. Vicente, J. Power Sources 227 (2013) 65.
[11] M.J. Aragón, B. León, C.P. Vicente, J.L. Tirado, Inorg. Chem. 47 (2008) 10366.
[12] W. Kang, Q. Shen, J. Power Sources 238 (2013) 203.
[13] W.A. Ang, N. Gupta, R. Prasanth, S. Madhavi, ACS Appl. Mater. Interfaces 4 (2012) 7011.
[14] Y. Zhong, L. Su, M. Yang, J. Wei, Z. Zhou, ACS Appl. Mater. Interfaces 5 (2013) 11212.
[15] Z. Ding, B. Yao, J. Feng, J. Zhang, J. Mater. Chem. A 1 (2013) 11200–11209.
[16] M.V. Reddy, G.V. Subba Rao, B.V.R. Chowdari, Chem. Rev. 113 (2013) 5364.
[17] T. Brezesinski, J. Wang, J. Polleux, B. Dunn, S.H. Tolbert, J. Am. Chem. Soc. 131 (2009) 1802.
[18] B.E. Conway, V. Birss, J. Wojtowicz, J. Power Sources 66 (1997) 1.
[19] L. Su, Y. Zhong, Z. Zhou, J. Mater. Chem. A (2013), http://dx.doi.org/10.1039/C3TA13233A.
[20] L. Shao, R. Ma, K. Wu, M. Shui, M. Lao, D. Wang, N. Long, Y. Ren, J. Shu, J. Alloys Compd. 581 (2013) 602.
[21] X. Ming, X.-L. Wang, F. Du, J.-W. Yin, C.-Z. Wang, G. Chen, J. Alloys Compd. 510 (2012) L1.
[22] Y. Ein-Eli, Electrochem. Solid-State Lett. 2 (1999) 212.
[23] Y. He, L. Huang, J.-S. Cai, X.-M. Zheng, S.-G. Sun, Electrochim. Acta 55 (2010) 1140.
[24] J. Morales, L. Sánchez, F. Martín, F. Berry, X. Ren, J. Electrochem. Soc. 152 (2005) A1748.
[25] J.K. Heuer, J.F. Stubbins, Corros. Sci. 41 (1999) 1231.
[26] J. Morales, J. Santos-Peña, R. Trócoli, S. Franger, E. Rodríguez-Castellón, Electrochim. Acta 53 (2008) 6366.
[27] V. Eshkenazi, E. Peled, L. Burstein, D. Golodnitsky, Solid State Ionics 170 (2004) 83.
[28] D. Yang, A. Velamakanni, G. Bozoklu, S. Park, M. Stoller, R.D. Piner, S. Stankovich, I. Jung, D.A. Field, C.A. Ventrice Jr., R.S. Ruoff, Carbon 47 (2009) 145.
[29] J. Shu, M. Shui, F. Huang, D. Xu, Y. Ren, L. Hou, J. Cui, J. Xu, J. Phys. Chem. C 115 (2011) 6954.